Real-Time Digital Twin for Construction Vehicle Stability Assessment and Visualization with Improved Front-Loader Payload Estimation

Théo Tuerlinckx[1][a], Sam Weckx[1][b], Steven Robyns[1][c] and Jeroen D. M. De Kooning[2,3][d]

[1]*MotionS Corelab, FlandersMake, 133 Oude Diestersebaan, 3920 Lommel, Belgium*

[2]*Department of Electromechanical, Systems and Metal Engineering, Faculty of Engineering and Architecture, Ghent University, Belgium*

3

{*theo.tuerlinckx, sam.weckx, steven.robyns*}*@flandersmake.be, jeroen.dekooning@ugent.be*

Keywords: Construction Vehicle, Digital Twin, Stability Assessment, Stability Visualization, Payload Estimation Method, Multibody Modelling.

Abstract: The stability assessment of construction vehicles, which are part of a constantly growing market, is of a high importance for safety and working efficiency. For such vehicles, the stability is mainly impacted by the carried payload. In this paper, a state of the art payload estimation method, based on simplified motion equations, is further improved by coupling it with accurate real-time multibody modelling. An example, that allows to reduce the important impact of joints damping on the payload estimation method, is developed and validated in this paper. A reduction of the payload estimation moving window root mean square error from 12.8% to 2.9% is obtained. Finally, the tractor multibody digital-twin is integrated in a real-time system on a physical setup, allowing to process the signals of the tractor and provide an easy to interpret visualization of the vehicle stability to the operator.

1 INTRODUCTION

The market of construction vehicles, such as bulldozers, excavators, tractors with front-loader, etc, is constantly growing because of the increase of construction activities due the expansion of the humanity (MarkwideResearch, 2024). This trend is also followed by an integration of Advanced Driver Assistance Systems (ADAS) to improve the safety and efficiency of those vehicles (AlliedMarketResearch, 2024). The main study concern in this paper is the stability of construction vehicles. Going towards more efficient construction means moving higher payloads at higher speeds. This payload, whose value and exact position are often unknown by the operator, can lead to instability of the vehicle and even rollover (Zhu et al., 2021). Additionally to the payload value and position, the vehicle suspension plays an important role for the vehicle stability while it is moving (Cordoş and TodoruŢ, 2019). However, this research is only focusing on the payload estimation impact on vehicle stability and not the suspension system.

A lot of research already focused on the analysis of stability behaviour in construction vehicles. (Mitrev and Marinković, 2019) is performing a full numerical study for the stability of an excavator, including the tire suspensions, while (Edwards et al., 2019) focuses on the risk of overturning. However, both are assuming a known payload. (Lysych, 2020) is using SolidWorks to study the dynamics of a tractor, including working tools at the front and rear of the vehicle, but without taking into account the movement of those tools. (Baker and Guzzomi, 2013) is analysing the stability of a tractor on a slope by including the effect of the front axle-wheel mass, underlining the important impact of it on the overall Center Of Gravity (COG) position but without including the impact of the front-loader and its payload. It can be seen that therefore most of the research about construction vehicle stability assumes a know payload or are not including the dynamics of the front-loader.

By looking at the state of the art in estimating payload, the research of (Ferlibas and Ghabcheloo, 2021), that will be further analysed in this paper, presents a novel approach for dynamic payload esti-

[a] https://orcid.org/0000-0001-9780-0714
[b] https://orcid.org/0000-0001-6983-495X
[c] https://orcid.org/0000-0001-5898-7061
[d] https://orcid.org/0000-0002-0358-4350

Tuerlinckx, T., Weckx, S., Robyns, S. and M. De Kooning, J. D.
Real-Time Digital Twin for Construction Vehicle Stability Assessment and Visualization with Improved Front-Loader Payload Estimation.
DOI: 10.5220/0013080500003941

In *Proceedings of the 11th International Conference on Vehicle Technology and Intelligent Transport Systems (VEHITS 2025)*, pages 266-277
ISBN: 978-989-758-745-0; ISSN: 2184-495X

mation on an excavator without including joints friction and damping. (Bennett et al., 2014) use a multibody model to study the impact of static and dynamic behaviour of an excavator on payload estimation methods in simulation. Moreover, a state estimator (Ishihara et al., 2021) or neural network (Huo et al., 2023) can also be used to estimate payload of construction vehicles. On the other side, other researchers are focusing on accurate and complex modeling of construction vehicles with multibody modeling (Pavlov and Dacova, 2021) or the finite element method (Gralak and Waluś, 2024), but also assume a known payload.

This paper aims to bridge the gap between simplified payload estimation methods and the accuracy of multibody modeling. It focuses on developing a digital twin of a tractor using Simscape Multibody, including the hydraulic front-loader and suspension systems. The digital twin is defined as a virtual replica that acts and behaves like its physical counterpart, with automated data transfer between the physical system and the virtual model. The multibody model is coupled with an adapted payload estimation method and validated through experimental tests on a physical tractor setup. The research highlights the potential to improve or analyze the stability of construction vehicles by coupling multibody modeling with payload estimation methods. It also presents an improved payload estimation method that is robust to joint damping, which can significantly impact construction vehicles. Finally, the digital twin is integrated into a real-time system on the physical setup, allowing for signal processing and 3D visualization of vehicle stability for the operator.

The paper is structured as follows. The second section describes the theory, models, and methods for tractor multibody modeling, payload estimation, and stability assessment. Section 3 details experiments validating these methods with field measurements. Finally, the Section 4 discusses the results and Section 5 provides a summary and outlook.

2 THEORY, MODELS AND METHODS

In order to validate the improvement on construction vehicle stability assessment and visualization, a relevant industrial case of a construction vehicle is used. A New Holland T7.175 SideWinder II tractor with a Still front loader 770TL is modelled as a multi-body model and used as real physical setup for data collection. The physical setup is also used to gather signals that will be used as input for the model such as the front-loader positions or hydraulic pressures. The tractor has a front-loader actuated by an hydraulic system with different possibilities of working implements (i.e. a bucket or a fork). The suspension system is made of a front-axle TerraGlide suspension developed by New Holland.

In order to assess the stability of the tractor, firstly, an estimation of the front-loader payload is calculated. Secondly, the tractor center of gravity is computed based on the weight distribution. Thirdly, the tractor stability is discussed, taking into account the influence of the tractor pitch. Finally the visualization of the tractor stability to the vehicle operator and the overall real-time implementation architecture are depicted. The following subsections describe the physical and simulated model and the real-time methods and architecture used for front-loader payload estimation and stability assessment and visualization.

2.1 Physical Setup

The T7.175 tractor physical setup can be seen in Figure (1). The setup is made of two main subsystems : the front-loader hydraulic system and the suspensions system, which are described in the section below.

Figure 1: Tractor physical setup.

2.1.1 Front-Loader Hydraulic System

The front-loader has two main degrees of freedom (DOF). The main arm (blue part in Figure (2)) rotates along the Y-axis relative to the tractor chassis (see yellow star in Figure (2)), and the implement (red part) rotates along the Y-axis relative to the arm tip (see red star). A hydraulic pump, driven by the tractor's engine, provides pressure and flow to the hydraulic cylinders (schematized as the yellow and red rectangle), which are part of a kinematic closed loop. This means the movements of the rotational DOFs are directly linked to the translational motions of the hydraulic cylinders.

Hydraulic flow is controlled by a lever, and the pump adjusts pressure based on the payload to achieve the desired movement. A system of valves maintains pressure in the hydraulic cylinders when the front-loader is stationary, allowing it to carry heavy loads without consuming power. Additionally, a payload stabilization system (green bar) ensures the implement remains stable when the main arm moves, preventing the payload from falling off by linking the two DOF's.

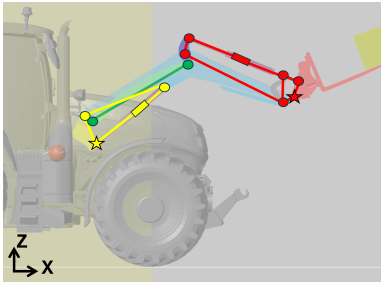

Figure 2: Front-loader degrees of freedom.

2.1.2 Suspensions System

The main suspension behavior of a tractor comes from the tire radial stiffness and damping that makes the connection between the chassis and the ground (Cuong et al., 2013). Additionally to this, a TerraGlide front-axle suspension system has been developed by NewHolland (New Holland Agriculture, 2024).

2.1.3 Sensors

The setup includes multiple sensors and an Industrial PC for processing sensor signals. Key components are:

- Leopard Imaging GMSL AR0231 camera: Estimates angles of the front-loader's main arm and implement using low cost vision methods (Robyns et al., 2024).
- PU501E pressure sensors: Measure pressure in both chambers of the hydraulic cylinders.
- Xsense MTi-30 Inertial Measurement Units (IMU): Provide roll and pitch measurements, with one unit on the chassis below the cabin and another on the front-axle below the suspension pivot point.

2.2 Simulation Multi-Body Model

A digital-twin of the tractor physical model is built in order to develop and validate the front-loader payload estimation and stability assessment as well as the visualization methods. The simulation model is implemented in the MATLAB environment, using the Simscape Multibody Library for simulating the tractor multi-body model while Simulink is used for post and pre-processing of the signals (e.g. computation of the hydraulic cylinder forces, payload estimation method, ...).

The Figure (3) shows the 3D visualization of the tractor Simscape Multibody model. The main chassis rigid body is imported as one CAD file while the two other subsystems, the suspensions and the front-loader hydraulics, are explained in more details in the following subsections.

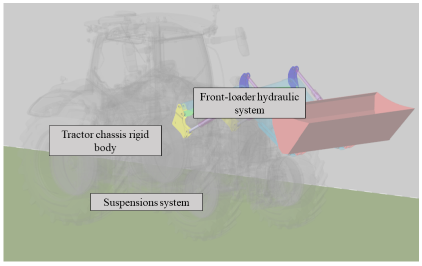

Figure 3: 3D visualization of the Tractor Simscape Multibody model with underlined subsystems.

2.2.1 Front-Loader Hydraulic System

The front-loader hydraulic system has two closed-loops for the main arm and implement on both sides, but only the right side is actuated in the simulation for simplicity. As the main arm and implement are modeled as rigid bodies, the left side of the model will follow the same movement. The kinematic close-loops are modeled in Simscape Multibody using prismatic and revolute joints, with one joint actuated by input and others automatically computed. The physical setup uses prismatic joints for actuation, while the simulation uses the revolute joints, demonstrating the benefits of a low-cost camera sensor for their position measurement (Robyns et al., 2024).

The front-loader payload estimation method requires the computation or measurement of torque in the DOF joints. In a Simscape Multibody model, this torque can be directly extracted from the revolute joints and is based on component inertias, payload, and front-loader movement. A virtual payload can be simulated by adding a variable mass component to the implement. However, in real industrial applications where the payload is unknown, the method must compute the joint's torque using regular sensors with the following approach.

Knowing the pressure in the hydraulic cylinders, their forces can be computed as the difference in force between the two chambers:

$$F = F_{Ch_A} - F_{Ch_B} \tag{1}$$

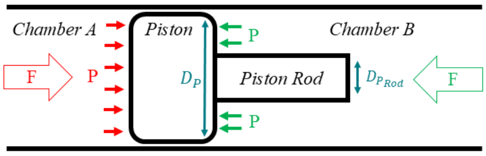

Figure 4: Hydraulic cylinder schematic.

with:

$$F = A \cdot P \tag{2}$$

With P the hydraulic pressure in *Pascal* and A the chamber bore area in m^2 (see Figure (4)):

$$A_{Ch_A} = \frac{\pi}{4} \cdot D_P^2 \tag{3}$$

and

$$A_{Ch_B} = \frac{\pi}{4} \cdot \left(D_P^2 - D_{P_{Rod}}^2\right) \tag{4}$$

Regarding the hydraulic pressure, this one is measured before the chambers. In order to account for the pressure loss in the hydraulic circuit between the sensors and the chambers (i.e. junction, bend, etc), the pressure measurement is multiplied by an efficiency factor:

$$P = P_m \cdot \eta_P \tag{5}$$

Once the hydraulic cylinder force is computed, it can be applied as an input force to the cylinder prismatic joint of the model. The Simscape Multibody model, by multiplying those forces with the cylinder jacobians, can directly extract the torque in the DOF revolute joints, knowing the hydraulic cylinder pressure and corresponding DOF's positions. The torques are computed with a multibody model with components with an infinitely small density and no payload in the implement as the hydraulic pressure measurement on the physical setup already includes those element effects.

2.2.2 Suspensions System

This subsystem is modelled and validated using the IMU's measurement with the tractor at standstill. However the rolling vehicle with acceleration and deceleration is not yet modelled. Therefore, the study of the impact of the suspension subsystem on the vehicle stability is not further investigated here.

2.2.3 Solver and Parameters Value

Simscape Multibody uses a fixed time step to solve the equations of motion for the mechanical system. Simulink systems (i.e. computation of the hydraulic cylinder force, payload estimation, etc.) use a fixed step solver (Bogacki–Shampine) for third-order ordinary differential equations. The time step allows real-time simulation, enabling integration into a physical setup for stability assessment and smooth visualization.

Finally, the overall parameter values of the multibody model are summarized in the Table (1).

Table 1: Tractor multibody-model parameters.

Parameters	Units	Value
ρ	kg/m^3	5500
$M_{Tractor}$	kg	6000
M	kg	10
$D_{Piston,Arm}$	m	0.1475
$D_{PistonRod,Arm}$	m	0.0381
$\eta_{P,Arm}$	$\%$	0.58
$D_{Piston,Implement}$	m	0.1079
$D_{PistonRod,Implement}$	m	0.0165
$\eta_{P,Implement}$	$\%$	0.69
a_2	m	2.97
I_{arm}	kgm^2	780.8
M_{arm}	kg	1320
α_3	rad	0.23
r_3	m	1.42
a_3	m	2.85
I_{imp}	kgm^2	34.59
M_{imp}	kg	272.7
α_4	rad	0.2663
r_4	m	0.4723
$C_{HC,Arm}$	$N/(m/s)$	3.9e+05
$C_{HC,Implement}$	$N/(m/s)$	1.15e+05
$Ts_{Simscape}$	s	1e-03
$Ts_{Simulink}$	s	1e-03

2.3 Front-Loader Payload Estimation

The front-loader payload estimation used within this paper is based on (Ferlibas and Ghabcheloo, 2021) and schematized in Figure (5). The front-loader can be considered as a three-revolute joint manipulator in the vertical plane with the tractor pitch, the main arm and the implement joint. The dynamic torque equations of that manipulator are rewritten in a decoupled form as the linear combination of dynamic gravitational parameters and functions of joint angles, velocities, and accelerations. A measurement campaign without payload on the physical setup can then be performed to measure the joint torques with their corresponding joint position and speed. A least squares estimation can then be used to identify the gravitational parameters for a joint configuration without payload. Therefore, when performing a measurement with payload, the relation between the actual with-load torque can be made with the estimated without-load torque using the gravitational parameters. From this relation, an estimation of the payload can be computed (Ferlibas and Ghabcheloo, 2021). The summarized method is now presented in more details.

As the front-loader can be considered as a three-revolute joint manipulator in the vertical plane, the dynamics can be described with the following equation (Ferlibas and Ghabcheloo, 2021):

$$\tau = D(\Theta)\ddot{\Theta} + C(\Theta,\dot{\Theta}) + G(\Theta) \tag{6}$$

With:

- τ: the joint torque vector
- Θ: the vector of joint angles
- $D(\Theta)$: the inertia matrix
- $C(\Theta,\dot{\Theta})$: the vector of Coriolis and centrifugal terms
- $G(\Theta)$: the gravity torque vector

And with the corresponding schematic diagram in Figure (6) where θ_2 is the pitch angle, θ_{23} the arm angle and θ_{234} the implement angle.

As explained above, the torque equation (6) can be rewritten in a decoupled form as the linear combination of dynamic gravitational parameters, π, and a matrix Y function of joint angles, velocities, and accelerations:

$$\tau = Y(\Theta,\dot{\Theta},\ddot{\Theta})\pi \tag{7}$$

By neglecting the friction and damping in the joints, the linear torque equations can be obtained using Euler-Lagrange method (Ferlibas and Ghabcheloo, 2021):

$$\begin{aligned}
\tau 4 = {} & (I_{imp} + M_{imp}r_4^2)\ddot{\theta}_{234} \\
& + M_{imp}a_2r_4[\ddot{\theta}_2 cos(\theta_{34}+\alpha_4) + \dot{\theta}_2^2 sin(\theta_{34}+\alpha_4)] \\
& + M_{imp}a_3r_4[\ddot{\theta}_{23} cos(\theta_4+\alpha_4) + \dot{\theta}_{23}^2 sin(\theta_4+\alpha_4)] \\
& + M_{imp}gr_4cos(\theta_{234}+\alpha 4) \\
\tau 3 = {} & \tau 4 + (I_{arm} + M_{arm}r_3^2 + M_{imp}a_2^3)\ddot{\theta}_{23} \\
& + M_{imp}a_2a_3[\ddot{\theta}_2 cos(\theta_3) + \dot{\theta}_2^2 sin(\theta_3)] \\
& + M_{imp}a_3r_4[\ddot{\theta}_{234}(\theta_4+\alpha_4) - \dot{\theta}_{234}^2 sin(\theta_4+\alpha_4)] \\
& + M_{arm}a_2r_3[\ddot{\theta}_2(\theta_3+\alpha_3) + \dot{\theta}_2^2 sin(\theta_3+\alpha_3)] \\
& + M_{imp}ga_3cos(\theta_{23}) + M_{arm}gr_3cos(\theta_{23}+\alpha_3)
\end{aligned} \tag{8}$$

With:

- I_{arm}, I_{imp}: the moments of inertia of the main arm and implement respectively
- M_{arm}, M_{imp}: the masses of the main arm and implement respectively
- a_2: the linear distance between the pitch joint and the arm joint
- a_3: the linear distance between the arm joint and the implement joint, also called the arm length in that paper.
- α,r: the polar coordinates of the center of gravity of the arm $_3$ and the implement $_4$.

Note that the torque equation of the pitch τ_2 has not been written as the pitch torque is not measured on the physical setup and therefore cannot be used.

2.3.1 Dynamic Estimation of the Payload

Now that the torque equations have been described, they can be rewritten in the matrix form of (7), (Ferlibas and Ghabcheloo, 2021):

$$\begin{bmatrix} \tau_4 \\ \tau_{34} \end{bmatrix} = \begin{bmatrix} y_{11} & 0 & y_{13} & y_{14} & 0 & 0 \\ 0 & y_{22} & y_{23} & y_{24} & y_{25} & y_{26} \end{bmatrix} \begin{bmatrix} \pi_{d1} \\ \pi_{d2} \\ \pi_{s1} \\ \pi_{s2} \\ \pi_{s3} \\ \pi_{s4} \end{bmatrix} \tag{9}$$

with $\tau_{34} = \tau_3 - \tau_4$ and:

$$\begin{aligned}
y_{11} &= \ddot{\theta}_{234} \\
y_{13} &= a_2\ddot{\theta}_2 cos(\theta_{34}) + a_2\dot{\theta}_2^2 sin(\theta_{34}) + a_3\ddot{\theta}_{23} cos(\theta_4) \\
&\quad + a_3\dot{\theta}_{23}^2 sin(\theta_4) + gcos(\theta_{234}) \\
y_{14} &= -a_2\ddot{\theta}_2 sin(\theta_{34}) + a_2\dot{\theta}_2^2 cos(\theta_{34}) - a_3\ddot{\theta}_{23} sin(\theta_4) \\
&\quad + a_3\dot{\theta}_{23}^2 cos(\theta_4) - gsin(\theta_{234}) \\
y_{22} &= \ddot{\theta}_{23} \\
y_{23} &= a_3\ddot{\theta}_{234} cos(\theta_4) - a_3\dot{\theta}_{234}^2 sin(\theta_4) \\
y_{24} &= -a_3\ddot{\theta}_{234} sin(\theta_4) - a_3\dot{\theta}_{234}^2 cos(\theta_4) \\
y_{25} &= a_2\ddot{\theta}_2 cos(\theta_3) + a_2\dot{\theta}_2^2 sin(\theta_3) + gcos(\theta_{23}) \\
y_{26} &= -a_2\ddot{\theta}_2 sin(\theta_3) + a_2\dot{\theta}_2^2 cos(\theta_3) - gsin(\theta_{23})
\end{aligned} \tag{10}$$

Using that set of linearized equations, the gravitational parameters π can be estimated using the Least Squares Estimation method with a set of measurements (without payload) of the joints torque without payload τ and joints position θ. As the joints velocity $\dot{\theta}$ and acceleration $\ddot{\theta}$ are not measured on the physical setup, their values are simplified as the derivatives of the position.

Thereafter, when adding a payload M_{pl} in the implement, assuming that the implement center of gravity is fixed and does not change depending on the variable load weight in the implement (Ferlibas and Ghabcheloo, 2021), the difference between the loaded arm torque τ_3 and the loaded implement torque τ_4 (i.e.

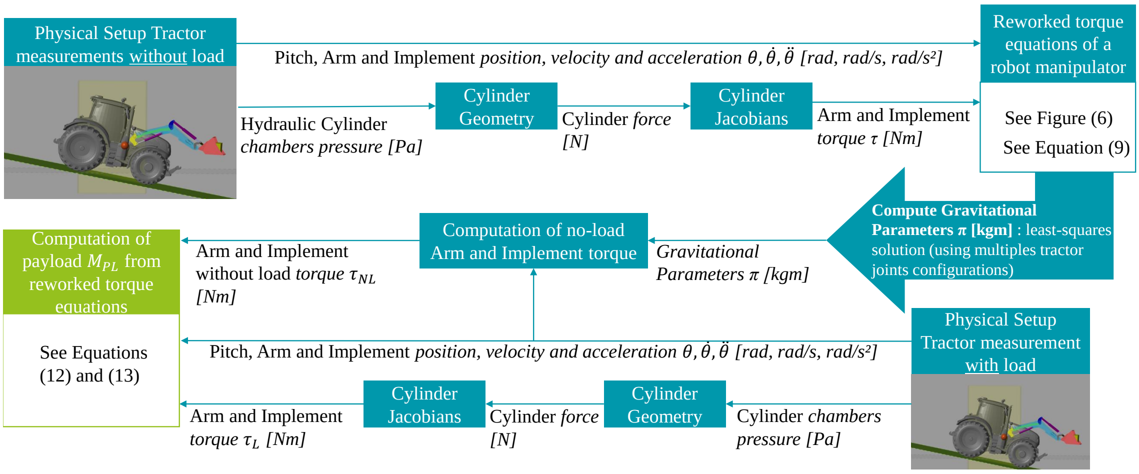

Figure 5: Front-loader payload estimation overall method.

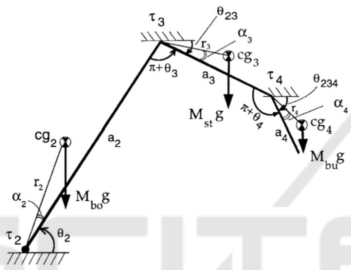

Figure 6: Three-revolute joint manipulator schematic diagram (Tafazoli et al., 1999).

$\tau_{34} = \tau_3 - \tau_4$) can be defined by replacing M_{imp} by $M_{imp} + M_{pl}$ in the equations (8):

$$\begin{aligned}
\tau_{L,34} = {} & (I_{arm} + M_{arm} r_3^2 + (M_{imp} + M_{pl}) a_2^3)\ddot{\theta}_{23} \\
& + (M_{imp} + M_{pl}) a_2 a_3 [\ddot{\theta}_2 cos(\theta_3) + \dot{\theta}_2^2 sin(\theta_3)] \\
& + (M_{imp} + M_{pl}) a_3 r_4 \ddot{\theta}_{234} (\theta_4 + \alpha_4) \\
& - (M_{imp} + M_{pl}) a_3 r_4 \dot{\theta}_{234}^2 sin(\theta_4 + \alpha_4) \\
& + M_{arm} a_2 r_3 [\ddot{\theta}_2 (\theta_3 + \alpha_3) + \dot{\theta}_2^2 sin(\theta_3 + \alpha_3)] \\
& + (M_{imp} + M_{pl}) g a_3 cos(\theta_{23}) \\
& + M_{arm} g r_3 cos(\theta_{23} + \alpha_3) \qquad (11)
\end{aligned}$$

That equation can be rewritten as the difference between the loaded torque $\tau_{L,34}$ (11) and a no-loaded torque $\tau_{NL,34}$ (8):

$$\begin{aligned}
\tau_{L,34} - \tau_{NL,34} = {} & M_{pl} a_2^3 \ddot{\theta}_{23} \\
& + M_{pl} a_2 a_3 [\ddot{\theta}_2 cos(\theta_3) + \dot{\theta}_2^2 sin(\theta_3)] \\
& + M_{pl} a_3 r_4 \ddot{\theta}_{234} (\theta_4 + \alpha_4) \\
& - M_{pl} a_3 r_4 \dot{\theta}_{234}^2 sin(\theta_4 + \alpha_4) \\
& + M_{pl} g a_3 cos(\theta_{23}) \qquad (12)
\end{aligned}$$

Finally, the payload estimation M_{pl} can be isolated as:

$$M_{pl} = \frac{\tau_{L,34} - \tau_{NL,34}}{\begin{array}{c} a_2^3 \ddot{\theta}_{23} + a_2 a_3 [\ddot{\theta}_2 cos(\theta_3) + \dot{\theta}_2^2 sin(\theta_3)] \\ + a_3 r_4 [\ddot{\theta}_{234} (\theta_4 + \alpha_4) - \dot{\theta}_{234}^2 sin(\theta_4 + \alpha_4)] \\ + g a_3 cos(\theta_{23}) \end{array}} \qquad (13)$$

Where, for a measured joints state $(\theta, \dot{\theta}, \ddot{\theta})$, $\tau_{L,34}$ is directly computed from the physical setup pressure measurements and $\tau_{NL,34}$ is estimated using the gravitational parameters and equations (9).

2.3.2 Robustness to Hydraulic Damping

As shown in the previous equations, the payload estimation method is not accounting for joints damping and friction in order to allow a linearisation of the torque equations. However, off-road vehicles are often working with robust joints actuated by hydraulics, therefore inducing a significant joints friction and damping, as it is observed on the physical setup measurement of Figure (10).

In order to improve the accuracy of the payload estimation, the hydraulic force computation presented in Section 2.2.1 is further adapted by reducing the effect of the damping[1]. For that, a damping force is subtracted to the force computed in (2):

$$F = A \cdot P - F_{damp} \qquad (14)$$

with:

$$F_{damp} = C_{HC} \cdot v_{HC} \qquad (15)$$

with C_{HC} the hydraulic cylinder damping coefficient and v_{HC} the hydraulic cylinder velocity in m/s. The

[1]The friction is not analysed within that research but can use a similar approach.

parameter C_{HC} can then be optimized in order to match the ideal torque from simulation (i.e. without damping) with the new adapted model as explained in Section 3.1 and validated in Section 4.1.

2.4 Stability Assessment and Visualization

Now that the unknown payload in the tractor front-loader has been estimated, the overall stability of the vehicle can be assessed. The tractor stability is mainly evaluated by its Center Of Gravity position. A tractor will remain stable as long as the overall COG stay in the tractor stability baseline delimited as the horizontal projection of the imaginary lines passing by the four wheel-ground contacts (Murphy, 2022):

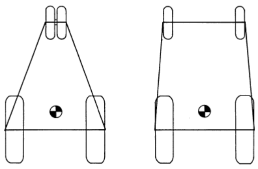

Figure 7: Tractor stability baseline (Murphy, 2022).

The tractor stability baseline is first defined by the tractor track width and wheel base, see Figure (7). However this baseline is also influenced by the tractor roll and pitch. As it can be seen on Figure (8), the horizontal projection of the lines passing by the two rear wheels is smaller in the right configuration, therefore reducing the stability area.

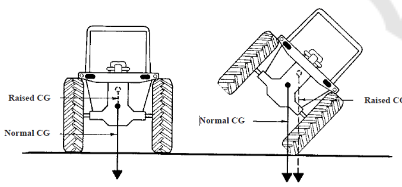

Figure 8: Influence of tractor stability baseline and COG position on stability assessment (Murphy, 2022).

Secondly the stability is influenced by the COG position. In the right configuration of Figure (8), the tractor with a raised COG becomes unstable as the point is going out of the stability baseline. From a physical point of view, it means that the roll moment of force around the right wheel-ground contact point will make the tractor roll over in the clockwise direction.

2.4.1 Center of Gravity Position Evaluation

Knowing the COG position is therefore of high importance to evaluate the tractor stability. The initial fixed COG position of the tractor can be directly computed from the tractor geometry and components weights, including additional working tools, counterbalancing weights, etc. However, during operation, the COG will also be impacted by the moving payload in the front-loader. For example, a heavy payload in a raised front-loader can lead to the unstable case depicted with raised COG in Figure (8).

In simulation, the following approach is used to evaluate the COG position. A first model is simulated, without payload in the implement and without components density. Using the hydraulic force measurement as input with the corresponding joint states, the payload is estimated as an output using the method from Section 2.3.1. Then a second model is used with the similar joint states, with component density and a virtual mass in the implement using the value from the first model output. Finally, the COG position can be extracted from that group of body elements using the Inertia Sensor block from Simscape Multibody.

2.4.2 Visualization Demonstration

It is essential to present the stability assessment to the vehicle operator in a manner that is intuitive and easy to interpret. Based on this visualization, the operator can evaluate whether adjustments to the planned vehicle trajectory are necessary or if additional measures, such as adding counterweights, are required to ensure stability. To facilitate the operator's understanding, a 3D visualization of the vehicle is preferred over purely numerical or graphical representations.

Furthermore, it is preferable for the operator to have access to a single, integrated visualization that consolidates various aspects of vehicle operation, rather than multiple, separate displays. This visualization should accommodate additional functionalities beyond stability assessment, such as monitoring vehicle component performance. A versatile solution is proposed using a gaming engine (Unreal Engine) which can easily be deployed as a standalone executable.

Coming back to the digital twin definition mentionned in Section 1, the visualization to the operator is here referring to the information flow from the virtual to physical system.

2.5 Real-Time Implementation Architecture

The described payload estimation method and stability assessment must be effectively integrated to ensure a real-time system in which (1) payload estimation and stability assessment are continuously updated based on sensor inputs, and (2) the resulting output is accurately visualized for the operator. This integration requires the coordination of multiple software tools—Matlab/Simulink/Simscape, Unreal Engine, and Python scripts for sensor data processing—among which data must be transmitted.

The complete system architecture is illustrated in Figure (9), where the multibody model and visualization components are highlighted in red and blue, respectively. The ROS (Robot Operating System) serves as the communication middleware within this architecture, facilitating data exchange between different software components, as indicated by the blue arrows in Figure (9).

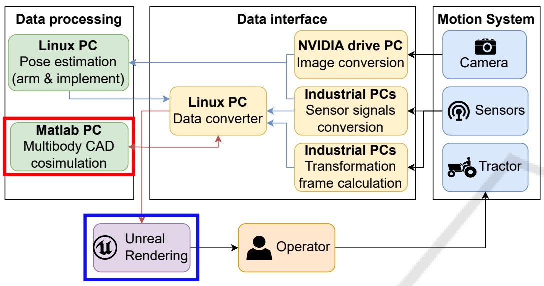

Figure 9: Real-time implementation architecture.

However, since communication between Simscape and ROS, as well as Unreal Engine and ROS, requires additional toolboxes or third-party plugins, the implementation instead utilizes UDP, indicated by the red arrows. UDP is preferred over TCP because it can tolerate occasional data loss, as it is solely intended for visualization purposes, where minimizing delays is critical for providing real-time feedback to the operator. Data centralization and conversion between ROS and UDP are managed by the "Data Converter" component.

3 EXPERIMENTS AND ASSUMPTIONS

As the setup, models and methods have been described in the previous section, this section focuses on the experiments executed as well as the assumptions used. In this research, four main models and methods need to be validated and are therefore listed in the following subsections.

3.1 Hydraulic System

The hydraulic model with reduced impact of damping is validated with the following experiment. The tractor is placed at standstill, a known payload $M_{pl} = 475kg$ is placed in the implement (i.e a bucket full of sandbags) and the front-loader is dynamically actuated with different positions while all the signals from sensors listed in the Section 2.1.3 are logged.
With a first simulation, the arm and implement joint torque can be extracted from a model without virtual payload and without component density but by using the hydraulic force measurement as input (see Section 2.2.1). Then a second simulation can be run using the similar joint states, a virtual known mass in the implement and component density. Therefore, in the second simulation, the ideal joint torque without damping and stiffness can be directly extracted for a given payload (and without using the hydraulic force input from the physical setup). In that way, the hydraulic model of the first simulation can be adapted with a damping force in order to match the ideal model of the second simulation.

3.2 Payload Estimation

First, a calibration measurement needs to be performed on the physical setup without payload and by applying a dynamic movement to the front-loader. Then a first model without virtual payload, without components density but using the hydraulic force measurement as input is simulated. From the joints torque computation of that model, the gravitational parameters of the payload estimation method can be extracted using the Least Squares Estimation method as explained in Section 2.3.1. The validation of the payload estimation method can then use a similar measurement as for the validation of the hydraulic system. The pressure and joints state measurement from the physical setup with a known payload $M_{pl} = 475kg$ are used as inputs for the payload estimation method that outputs an estimated value of the payload overtime $\hat{M}$. The mean of the estimation error in percent can be expressed as following:

$$\bar{E} = 100 \cdot \underset{t\varepsilon[T_0,T_{end}]}{mean} \left| \frac{\hat{M} - M_{pl}}{M_{pl}} \right| \tag{16}$$

In order to reduce the error caused by unmodeled dynamic effects, a moving Root Mean Square (RMS) value of the payload estimation can be computed such that an operator of the tractor can have a steady estimation of the payload in real-time. The moving RMS value is computed as follow during the simulation:

$$\hat{M}_{MvRMS} = \sqrt{\underset{t\varepsilon T_{Window}}{mean} (\hat{M}^2)} \tag{17}$$

With $T_{Window} = 10s$ the time of the moving window.

Finally the overall error of the moving window value can be expressed in an error in percent as for $\hat{M}$:

$$\bar{E}_{MvRMS} = 100 \cdot \underset{t \varepsilon [T_0, T_{end}]}{mean} \left| \frac{\hat{M}_{MvRMS} - M_{pl}}{M_{pl}} \right| \quad (18)$$

3.3 Stability Assessment and Visualization

To assess the tractor stability, the stability baseline and COG position need to be evaluated. Regarding the stability baseline, this one can be easily extracted from the physical setup or simulation knowing the wheels position and the tractor roll and pitch. Therefore, an accurate estimation of the roll and pitch from IMU measurement leads to an accurate estimation of the stability baseline. Although, regarding the COG position, this one is more difficult to measure on the physical setup as it requires to know the weight distribution on the wheels in different vehicle roll-pitch positions. It was therefore not possible to validate the COG position with physical measurement. Nevertheless, the COG position is first impacted by the overall components CAD files accuracy, densities and the accuracy of their respecting COG position computation, which is not part of this research. Secondly, the overall COG is impacted by the front-loader position and the payload in its implement. The accuracy of the overall COG position is therefore assumed to be directly linked to the accuracy of the payload estimation discussed in the Section 4.2. For the purposes of visualization, it was assumed that the COG moves only in the forward and upward directions, while remaining centrally positioned along the vehicle's width. Consequently, the stability assessment is focused solely on potential tip-over in the pitch direction. As a result, a side view is deemed sufficient for operator visualization, and a front view—highlighting any asymmetry across the vehicle's width—is not necessary.

4 RESULTS AND DISCUSSIONS

4.1 Hydraulic System

The results of the first experiment, described in Section 3.1, are shown in the following figure:

The first graph shows the movement of the arm and the implement in function of the time. The graph bellow shows the computation of the arm revolute joint torque for three different models: the torque with damping directly computed from the setup pressure measurements in blue, the ideal torque without damping computed from simulation with a virtual mass

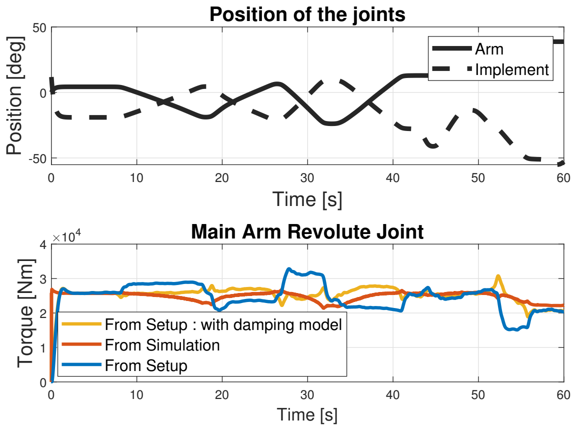

Figure 10: Calibration of Hydraulic Cylinder damping force model.

in orange and the new torque with reduced damping from the damping model also computed with the setup measurements in yellow. It can be observed that the curve with the damping model is not yet perfectly matching the ideal torque from simulation but is already closer than the initial model without damping force when the front-loader is moving. It is due to the fact that the complexity of the physical model, including several joints damping and friction, is simplified as one damping force on the hydraulic cylinder joint. Section 4.2 will show the improvement made on the payload estimation in dynamic condition using the damping reduction approach. The new optimized hydraulic damping parameters are listed in Table 1.

4.2 Payload Estimation

The improvement made in the hydraulic force computation of the previous section is now linked to the improvement on the payload estimation in the following graph:

The first graph is again showing the arm and implement position as well as the tractor pitch. In that experiment the tractor was placed on a flat area without pitch. In the second graph the estimated payload $\hat{M}$ from the initial model (in blue) and the model with reduced impact of the damping (in yellow) are compared to the actual value M_{pl} (in black). Both models are giving a good accuracy when the joints are at steady state. However, when the front-loader is dynamically excited, the method with damping model is giving a more stable estimation because of the reduced impact of the damping that is unmodeled in the payload estimation method. In that experiment, the mean of the estimation error in percent $\bar{E}$ is reduced from 16.1% to 5.9% and $\bar{E}_{MvRMS}$ from 12.8% to 2.9%.

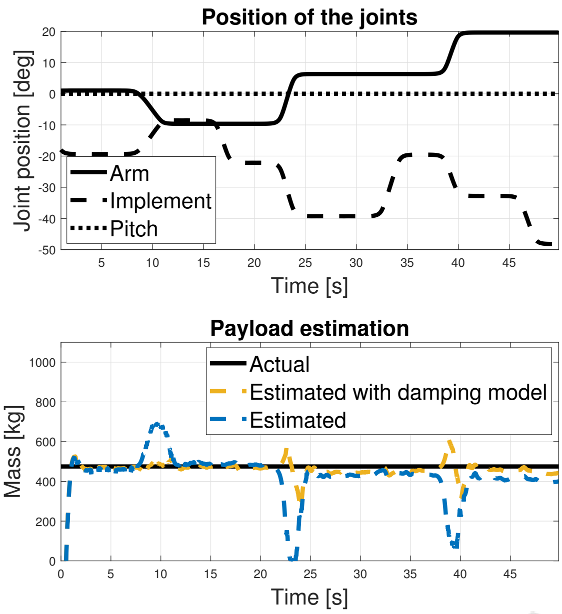

Figure 11: Payload estimation: comparison with the damping model.

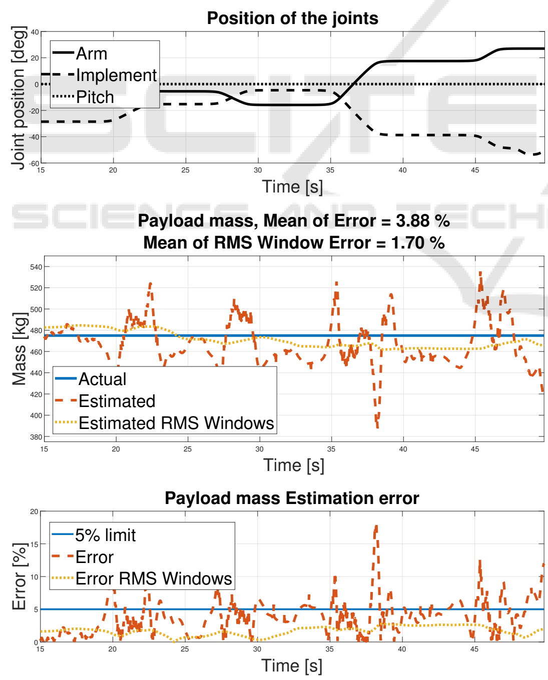

Figure 12: Payload estimation overtime.

The payload estimation of the model with reduced damping can be analysed in more details with an other set of data. Here, in the Figure (12), the estimated payload $\hat{M}$ and the estimated moving RMS value $\hat{M}_{MvRMS}$ are compared to the actual mass M_{pl}. The third graph displays the absolute error in percent of those two estimated quantities and a threshold of 5%. The estimated value is again giving a good accuracy with an error smaller than 5% with the joints at steady-state. However, when the front-loader is moving, a higher error is still remaining because the improved model has not fully removed the impact of the damping as underlined in Section 4.1. However, it is shown here that using the moving window RMS value can drastically reduce the impact of those unmodeled dynamics. The window RMS error value stays below 5% over the full experiment and has an average value of 1.7% versus 3.9% for the absolute value. If the payload in the implement of the construction vehicle is not expected to dynamically change over time once the vehicle is loaded, taking an average or a moving window RMS value is a good solution to deal with more complex unmodelled dynamic effects. Otherwise, the method with reduced damping shows an advantage for the case when the payload is constantly changing and moving. For example, an excavator that is digging a hole. The operator should not necessarily immobilize the front loader in order to check the payload value, therefore improving the productivity.

Table 2: Payload estimation results for multiple values.

M_{pl} [kg]	$\bar{\hat{M}}$ [kg]	$\bar{E}$ [%]	$\bar{\hat{M}}_{MvRMS}$ [kg]	$\bar{E}_{MvRMS}$ [%]
0	2	∞	17	∞
100	115	19.56	109	15.49
200	207	6.96	206	4.40
475	467	3.88	471	1.70

Finally, the overall approach is validated with multiple payload values. The Table (2) shows the mean of the estimated mass $\bar{\hat{M}}$ and moving RMS mass $\bar{\hat{M}}_{MvRMS}$ with the corresponding errors. While taking a moving RMS value is still improving the estimation, the accuracy decrease with the payload value. The error in percent is increasing for small payload, however the absolute error stay bellow 15kg A smaller payload estimation is more sensitive to the unmodelled dynamic effects but also to the accuracy of the pressure measurements, already including the mass of the front loader relatively high with respect to a small payload. However, small payload are less likely to lead to a vehicle instability while the estimation for high payload, between 500kg and 1500kg for a tractor front-loader, is expected to be acceptable.

4.3 Stability Assessment and Visualization

As introduced in the Section 3.3, the stability of a construction vehicle can be correctly assessed with an accurate estimation of the stability baseline, the COG position and the suspension system. Regarding the stability baseline, this one can be evaluated using an IMU measurement. Secondly, the COG position accuracy is here linked to the accuracy of the payload estimation presented in Section 4.2.

Figure 13: Visualization towards the operator.

Figure (13) presents the visualization provided to the operator. It displays the vehicle's center of gravity (COG), which shifts when the payload changes or when the tractor adjusts its implement. The yellow-shaded area represents the stability zone, defined as the projection of the stability baseline (as discussed in Section 4.3) along the direction of gravity. When the COG approaches the boundary of this area, it turns red, signaling an unstable condition and a heightened risk of tipping. In addition, the visualization includes numerical metrics, most notably the estimated payload and the remaining allowable weight before instability is reached.

5 CONCLUSION

This paper presents the overall story of improvement of construction vehicle stability assessment and visualization by coupling a front-loader payload estimation method with real-time multibody modeling. The main goal was to show that the accuracy of multibody modelling, for example with MATLAB Simscape Multibody software, can be used to improve a payload estimation method based on simplified motion equations. This paper underlines those improvements by reducing the impact of joints damping on the payload estimation and by allowing to run in parallel and in real-time a multibody model including suspensions system and Center Of Gravity computation.

Regarding the payload estimation, the multibody model is used to reduce the impact of joint damping by comparing joints torque from a physical setup and the ideal joint torque without damping in simulation. It therefore allows to quantify the impact of damping and remove it from the physical setup joint torque used for the payload estimation. The mean of the estimation moving window RMS error can be reduced from 12.8% to 2.9%. For real-time integration on a working vehicle, using such a solution with reduced impact of damping is better than just taking a mean on a moving windows value for vehicles that are constantly in movement or constantly changing the payload (e.g. a excavator digging an hole or moving sand).

The payload estimation and stability assessment have been integrated in a real-time system with a 3D visualization that is designed to provide the vehicle operator with intuitive feedback on stability, focusing on tip-over risks in the pitch direction. Communication between system components was achieved primarily through ROS and UDP. The system effectively visualizes the vehicle's center of gravity, stability zone, and key metrics, allowing operators to monitor and maintain safe operational conditions.

5.1 Outlook

The aims of this paper is to introduce a way to couple accurate multibody modelling with a more simplified payload estimation method using motion equations and integrate it in a real-time system with a 3D visualization. While some examples are demonstrated and validated within this research, several other investigations and modelling improvement could be further explored. First, the modelling of a moving vehicle could be developed. It allows to validate the impact of suspension on the stability behaviour but could also be used to improve the payload estimation method by reducing the impact of vehicle roll and pitch in case no IMU's measurements are available. Moreover, adding weight distribution measurement on the wheels of the physical setup could allow a more accurate validation of the center of gravity position and overall stability assessment. Finally, the payload estimation method could be further improved by modelling and reducing the impact of other unmodelled effects in the simplified motion equations such as joint frictions, hydraulics delay, components flexibility, etc.

ACKNOWLEDGEMENTS

This research is part of the CADAIVision SBO project funded and supported by Flanders Make vzw, the strategic research center for the manufacturing industry.

REFERENCES

AlliedMarketResearch (2024). Construction vehicles market size, share, competitive landscape and trend analysis report, by solution, by equipment, by type, by application and, by industry : Global opportunity analysis and industry forecast, 2023-2032. *Construction Vehicles Market*.

Baker, V. and Guzzomi, A. L. (2013). A model and comparison of 4-wheel-drive fixed-chassis tractor rollover during phase i. *Biosystems Engineering*, 116(2):179–189.

Bennett, N., Walawalkar, A., and Schindler, C. (2014). Payload estimation in excavators: Model-based evaluation of current payload estimation systems.

Cordoş, N. and TodoruŢ, A. (2019). Influences of the suspensions characteristics on the vehicle stability. In Burnete, N. and Varga, B. O., editors, *Proceedings of the 4th International Congress of Automotive and Transport Engineering (AMMA 2018)*, pages 808–813, Cham. Springer International Publishing.

Cuong, D., Zhu, S., Hung, D., and Ngoc, N. (2013). Study on the vertical stiffness and damping coefficient of tractor tire using semi-empirical model. *Hue University Journal of Science*, 83:5–15.

Edwards, D., Parn, E. A., Sing, M. C., and Thwala, W. D. (2019). Risk of excavators overturning: Determining horizontal centrifugal force when slewing freely suspended loads. *Engineering, construction, and architectural management*, 26(3):479–498.

Ferlibas, M. and Ghabcheloo, R. (2021). The 17th scandinavian international conference on fluid power. *Hue University Journal of Science*.

Gralak, M. and Waluś, K. (2024). A model of an extending front loader. *Applied Sciences*, 14:3948.

Huo, D., Chen, J., Zhang, H., Shi, Y., and Wang, T. (2023). Intelligent prediction for digging load of hydraulic excavators based on rbf neural network. *Measurement*, 206:112210.

Ishihara, S., Kanazawa, A., and Narikawa, R. (2021). Realization of excavator loading operation by nonlinear model predictive control with bucket load estimation. In *IFAC-PapersOnLine*, volume 54, pages 20–25. Elsevier Ltd.

Lysych, M. N. (2020). Study driving dynamics of the machine-tractor unit on a virtual stand with obstacles. *Journal of Physics: Conference Series*, 1515(4):42079–.

MarkwideResearch (2024). Construction vehicles market analysis- industry size, share, research report, insights, covid-19 impact, statistics, trends, growth and forecost 2024-2032. *Automotive and Transportation*, pages 1–263.

Mitrev, R. and Marinković, D. (2019). Numerical study of the hydraulic excavator overturning stability during performing lifting operations. *Advances in mechanical engineering*, 11(5):168781401984177–133.

Murphy, D. (2022). Tractor Stability and Instability. https://extension.psu.edu/tractor-stability-and-instability. Updated : July 15, 2022.

New Holland Agriculture (2024). Front Axle and Suspension. https://agriculture.newholland.com/apac/th-th/equipment/products/agricultural-tractors/t7-heavy-duty/detail/front-axle-and-suspension. Accessed: 2024-08-06.

Pavlov, N. and Dacova, D. (2021). A multibody model of a wheel loader with pneumatic boom suspension and proving ground testing. *IOP Conference Series: Materials Science and Engineering*, 1031:012009.

Robyns, S., Heerwegh, W., and Weckx, S. (2024). A digital twin of an off highway vehicle based on a low cost camera. *Procedia Computer Science*, 232:2366–2375. 5th International Conference on Industry 4.0 and Smart Manufacturing (ISM 2023).

Tafazoli, S., Lawrence, P. D., and Salcudean, S. E. (1999). Identification of inertial and friction parameters for excavator arms. *IEEE Trans. Robotics Autom.*, 15:966–971.

Zhu, Q., Yang, C., Hu, H., and Wu, X. (2021). Building a novel dynamics rollover model for critical instability state analysis of articulated multibody vehicles. *International Journal of Heavy Vehicle Systems*, 28:329–352.